

# Effect of ozone addition and ozonolysis reaction on the detonation properties of $C_2H_4/O_2/Ar$ mixtures

Jie Sun<sup>a</sup>, Baolin Tian<sup>b,a</sup>, Zheng Chen<sup>a,\*</sup>

<sup>a</sup> CAPT, SKLTCS, College of Engineering, Peking University, Beijing 100871, China

<sup>b</sup> LCP, Institute of Applied Physics and Computational Mathematics, Beijing 100094, China

Received 4 January 2022; accepted 2 September 2022

Available online 22 October 2022

## Abstract

Ozone is one of the strongest oxidizers and can be used to enhance detonation. Detonation enhancement by ozone addition is usually attributed to the ozone decomposition reaction which produces reactive atomic oxygen and thereby accelerates the chain branching reaction. Recently, ozonolysis reaction has been found to be another mechanism to enhance combustion for unsaturated hydrocarbons at low temperatures. In this study, the effects of ozone addition and ozonolysis reaction on steady detonation structure and transient detonation initiation and propagation processes in  $C_2H_4/O_2/O_3/Ar$  mixtures are examined through simulations considering detailed chemistry. Specifically, the homogeneous ignition process, the ZND detonation structure, the transient direct detonation initiation, and pulsating instability of one-dimensional detonation propagation are investigated. It is found that the homogeneous ignition process consists of two stages and the first stage is caused by ozonolysis reactions which consume  $O_3$  and produces  $CH_2O$  as well as H and OH radicals. The ozonolysis reaction and ozone decomposition reaction can both reduce the induction length though they have little influence on the Chapman–Jouguet (CJ) detonation speed. The supercritical, critical and subcritical regimes for direct detonation initiation are identified by continuously decreasing the initiation energy or changing the amount of ozone addition. It is found that direct detonation initiation becomes easier at larger amount of ozone addition and/or larger reaction progress variable. This is interpreted based on the change of the induction length of the ZND detonation structure. Furthermore, it is demonstrated that the ozonolysis reaction can reduce pulsating instability and make the one-dimensional detonation propagation more stable. This is mainly due to the reduction in activation energy caused by ozone addition and/or ozonolysis reaction. This work shows that both ozone decomposition reaction and ozonolysis reaction can enhance detonation for unsaturated hydrocarbon fuels.

© 2022 The Combustion Institute. Published by Elsevier Inc. All rights reserved.

**Keywords:** Detonation; Ozone; Ozonolysis reaction; Detonation initiation; Pulsating instability

## 1. Introduction

Detonation is a supersonic combustion wave, in which a leading shock wave is supported by a following reaction zone. Due to its advantages

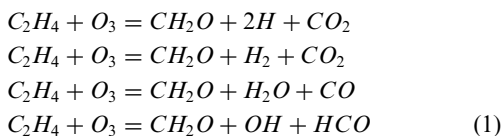
\* Corresponding author.

E-mail address: [cz@pku.edu.cn](mailto:cz@pku.edu.cn) (Z. Chen).

in achieving high thermal efficiency, fast heat release rate, and compact structure, detonation has promising applications in advanced propulsion systems [1]. In detonation engines, stable and controllable detonation needs to be maintained.

As one of the strongest oxidizers, ozone can be used to enhance/control detonation [2]. For examples, Shi et al. [3] assessed the effects of ozone addition on detonation structure in  $H_2/O_2$  mixtures. They found that ozone addition can greatly reduce the induction length and detonation cell size. Sepulveda et al. [4] found that a small amount of ozone addition can accelerate the deflagration to detonation transition (DDT) in  $C_2H_2/O_2$  mixtures. Han et al. [5, 6] demonstrated the potential of ozone sensitization to reduce the pulsating and cellular instabilities of detonation propagating in  $H_2/O_2$  mixtures. Kumar et al. [7] studied the effects of ozone addition on the detonation structure in  $H_2/air$  and  $C_2H_4/air$  mixtures and found that ozone addition can greatly reduce the induction length and extend the detonation propagation limits.

Usually, detonation enhancement by ozone addition is attributed to the ozone decomposition reaction which produces reactive atomic oxygen and thereby accelerates the chain branching reactions [2]. Recently, ozonolysis reaction [8, 9] has been found to be another mechanism to enhance combustion for unsaturated hydrocarbons at low temperatures. For example, the ozonolysis reactions for ethylene are [2]



The above ozonolysis reactions take place at room temperature, and produce radicals, such as H and OH, and intermediate component,  $CH_2O$ , which can greatly accelerate the subsequent chain reactions. The above process has been observed in experiments [10].

Therefore, the combustion process of unsaturated hydrocarbon fuels may be regulated by ozone addition. Gao et al. [10] investigated the ozonolysis activated autoignition in non-premixed coflow and found that ozonolysis reaction-induced autoignition does occur at room temperature and plays an important role in flame stabilization. Gao et al. [11] also found that the rapid ozonolysis reactions of  $C_2H_4$  at room temperature affect the laminar flame speed measurement for  $C_2H_4/air/O_3$  mixtures. Sun et al. [2] reviewed recent studies on the kinetics and dynamics involved in the effects of ozone addition on combustion. They found that ozone addition can greatly shorten the ignition delay time of  $C_2H_4/air$  mixtures, which is caused by ozonolysis reaction at low temperature ( $T < 700$  K) and ozone decomposition reaction at high temperature ( $T > 700$  K). Reuter et al. [12] assessed the effects

of ozone addition on the laminar burning velocity of  $CH_4/C_2H_4/air$  mixtures and found that ozonolysis reaction occurring in the upstream of the flame front greatly changes the laminar burning velocity.

However, ozonolysis reaction was only considered for ignition and premixed/non-premixed flames. Currently, there is no study assessing the effects of ozonolysis reaction on detonation process. In previous studies [3–7] on detonation promotion by ozone addition, the ozonolysis reaction was neglected and thereby it is not clear how ozonolysis reaction affects detonation. This motivates the present study, which aims to assess the effects of ozone addition and ozonolysis reaction on steady detonation structure and transient detonation initiation and propagation processes. Due to short half-life of ozone [13] and fast reaction rate constant between ozone and unsaturated hydrocarbon [2, 10] at room temperatures, it is difficult to obtain unreacted alkene/ozone mixtures. Nevertheless, as a potential method to regulate detonation initiation and propagation, partially premixed ozone/unsaturated hydrocarbon mixtures can be acquired and thereby it is necessary to assess the effects of ozonolysis reactions on detonation initiation and propagation. As a typical unsaturated hydrocarbon, ethylene is usually used as fuel in detonation studies since it has high reactivity and is the major component in the pyrolysis products of most hydrocarbon fuels [14]. Therefore, here we consider  $C_2H_4/O_2/Ar$  mixtures with ozone addition.

The paper is organized as follows. First, the model and numerical methods are introduced in Section 2. Then the effects of ozone addition and ozonolysis reaction on homogeneous ignition, one-dimensional ZND detonation structure, direct detonation initiation, and pulsating instability are examined in Section 3. Finally, the conclusions are presented in Section 4.

## 2. Model and numerical methods

We consider the homogeneous ignition process, ZND detonation structure, and direct detonation initiation in stoichiometric  $C_2H_4/O_2/O_3/Ar$  mixtures initially at  $T_0 = 300$  K. To avoid the interaction among complex oscillation modes on the analysis of results, the pressure of fresh mixtures is set to  $P_0 = 0.25$  atm so that only simple oscillation mode exists during the pulse detonation wave propagation process. The molar fraction for each species is determined by

$$\begin{aligned} X_{C_2H_4} : X_{O_2} : X_{O_3} &= (1 + 0.5a) : (3 - 3a) : 3a \\ X_{Ar} = 70\% &= 1 - X_{C_2H_4} - X_{O_2} - X_{O_3} \end{aligned} \quad (2)$$

where  $a$  is the molar/volumetric fraction of ozone in the oxidizer. The reduced mechanism for ethylene oxidation [15] and ozone sub-kinetic model including ozonolysis reactions [11, 16] are compiled

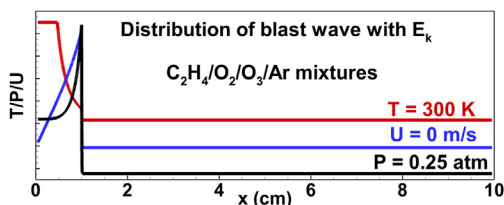


Fig. 1. Schematic of initial temperature, pressure and velocity distributions for 1D direct detonation initiation.

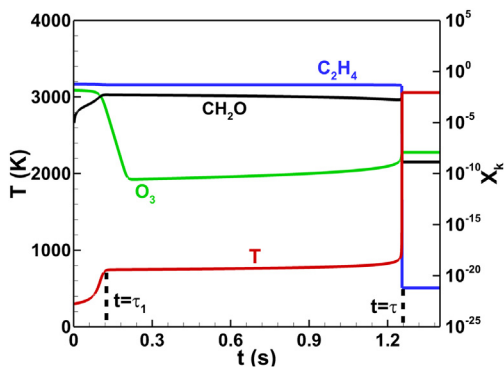


Fig. 2. Temporal evolution of temperature and molar fractions of  $C_2H_4$ ,  $CH_2O$  and  $O_3$  during the homogeneous ignition process in  $C_2H_4/O_2/O_3/Ar$  with  $a = 0.05$ ,  $P_0 = 0.25$  atm and  $T_0 = 300$  K.

together and used in all simulations. It is noted that further efforts need to be devoted to the validation of the kinetic model especially for the ozonolysis reactions. Nevertheless, the conclusions of this study are expected to be only quantitatively affected by the accuracy of the ozonolysis pathway reaction rates.

Cantera [17] is used to simulate the homogeneous ignition process in  $C_2H_4/O_2/O_3/Ar$  mixtures. The steady ZND structures for  $C_2H_4/O_2/Ar$  mixtures with different amounts of ozone addition and different reaction progress variables (defined later in Section 3.2) are simulated using SDtoolbox [18].

As depicted in Fig. 1, the Taylor-Sedov blast wave model [19, 20] is used as the initial condition in  $0 \leq x \leq 1$  cm to initiate the detonation. Note that a cutoff temperature of 9000 K and the corresponding density in the Taylor-Sedov solution were chosen since it is unreasonable to evaluate thermal properties for very high temperature (in fact the thermal properties are accurate only for temperature below 5000 K and linear extrapolation is used in A-SURF for temperature between 5000 K and 9000 K). The cutoff temperature of 9000 K is chosen somewhat arbitrary. Nevertheless, the same cutoff temperature is used for all simulations so that the comparison among difference cases is meaningful. The remaining region consists of  $C_2H_4/O_2/O_3/Ar$  mixtures at  $P_0 = 0.25$  atm and

$T_0 = 300$  K. The transient direct detonation initiation and propagation processes are simulated using A-SURF [21–23], which solves the conservation equations for transient, compressible, reactive flow using the finite volume method. A-SURF has been successfully used in previous studies on detonation initiation and propagation (e.g., [24–26]). The details on governing equations, numerical methods and code validation can be found in Refs. [21–23]. To efficiently and accurately resolve detonation initiation and propagation, adaptive mesh refinement is adopted in simulations. The basis grid size is 1 mm and the finest grid size is  $1.95 \mu m$ . The induction zone is covered by more than 40 grids, and grid convergence is ensured.

### 3. Results and discussion

#### 3.1. Homogeneous ignition

To understand how ozone addition and ozonolysis reaction affect the oxidation of ethylene, we first consider the homogeneous ignition. The results for ozone addition of  $a = 0.05$  are shown in Fig. 2.

Fig. 2 shows that the ignition process consists of two stages. The first-stage ignition is caused by ozonolysis reactions list in Eq. (1), which consume  $O_3$  and produces  $CH_2O$  as well as H and OH radicals. The temperature rises to around 746 K after the first-stage ignition. After a relatively long induction period, the second-stage ignition happens and  $C_2H_4$  and  $CH_2O$  are almost completely consumed. The temperature reaches to the equilibrium value of 3058 K. The global ignition delay time,  $\tau$ , and the first-stage ignition delay time,  $\tau_1$ , are indicated by the vertical dashed lines in Fig. 2. The global ignition delay time is defined based on the maximum temperature gradient while the first-stage ignition delay time is determined based on the peak of  $CH_2O$  molar fraction.

The effects of ozone addition on the homogeneous ignition process are further shown in Fig. 3. With the increase of ozone addition, both  $\tau_1$  and  $\tau$  decrease while their difference quickly decays. When  $a > 0.07$ , the second-stage ignition occurs immediately after the first-stage ignition, and thereby  $\tau \approx \tau_1$ . This is because both temperature and  $CH_2O$  molar fraction at the end of the first-stage ignition increase with ozone addition (see Fig. 3), which greatly accelerates the second-stage ignition.

The above results indicate that a small amount of ozone addition and the ozonolysis reaction at low temperature have great impact on the homogeneous ignition process. Therefore, they are expected to affect the detonation structure and direct detonation initiation process, which shall be shown below.

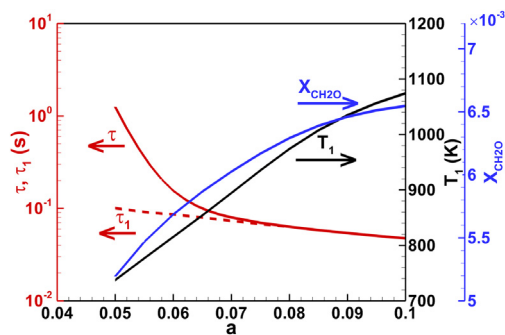


Fig. 3. Effects of ozone addition on the global and first-stage ignition delay time, and the temperature and  $\text{CH}_2\text{O}$  molar fraction,  $T_1$  and  $X_{\text{CH}_2\text{O}}$ , at the end of the first-stage ignition in  $\text{C}_2\text{H}_4/\text{O}_2/\text{O}_3/\text{Ar}$  mixtures at  $P_0 = 0.25$  atm and  $T_0 = 300$  K.

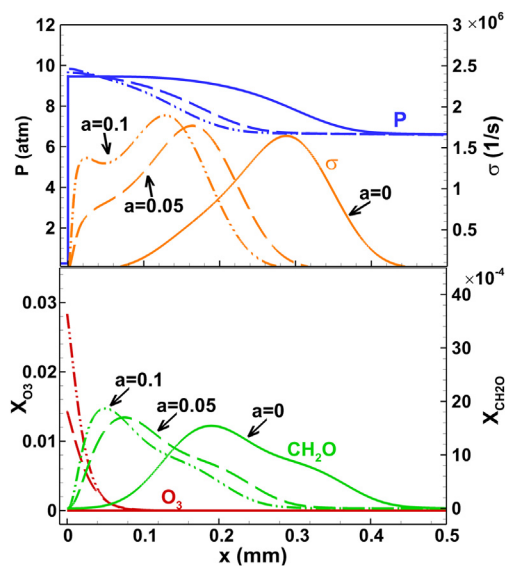


Fig. 4. Profiles for pressure,  $P$ , thermicity,  $\sigma$ , and  $\text{O}_3$  and  $\text{CH}_2\text{O}$  molar fractions,  $X_{\text{O}_3}$  and  $X_{\text{CH}_2\text{O}}$ , in the ZND detonation structure of  $\text{C}_2\text{H}_4/\text{O}_2/\text{O}_3/\text{Ar}$  mixtures at  $P_0 = 0.25$  atm and  $T_0 = 300$  K. The results for different amounts of ozone addition,  $a = 0, 0.05$  and  $0.1$ , are plotted together.

### 3.2. ZND detonation structure

The influence of ozone addition on the ZND detonation structure for  $\text{C}_2\text{H}_4/\text{O}_2/\text{Ar}$  mixtures are shown in Fig. 4. The leading shock locates at  $x = 0$  mm and the induction length is determined by the position of peak thermicity. When there is no ozone addition ( $a = 0$ ), the peak thermicity appears at  $x = 0.29$  mm. In the induction zone,  $\text{CH}_2\text{O}$  is first produced and then gradually consumed. As shown by the thermicity distribution, there is a relative broad reaction zone after the lead-

ing shock. For ozone addition of  $a = 0.05$ , the induction length reduces to  $L = 0.16$  mm, which is about half of the induction length  $L = 0.29$  mm for  $a = 0$ . Besides, the thermicity curve indicates that there is an exothermic region immediately after the leading shock, in which  $\text{O}_3$  is consumed and  $\text{CH}_2\text{O}$  is generated. When ozone addition further increases to  $a = 0.1$ , Fig. 4 shows that double peaks appear in the thermicity profile. Double peaks in the thermicity profile indicates that there are two characteristic induction lengths due to two-stage heat release. Such behavior affects the detonation dynamics, especially the multi-dimensional detonation cell structure. For example, double detonation cellular structure was observed in  $\text{NO}_2/\text{N}_2\text{O}_4$ -fuel mixtures [27] due to the two-stage heat release behind the leading shock. The cellular structure for detonation in  $\text{C}_2\text{H}_4/\text{O}_2/\text{O}_3/\text{Ar}$  mixtures needs to be explored in future studies. Note that the temperature after the leading shock is well above 2000 K, at which the ozone decomposition reaction dominates and ozonolysis reaction plays little role. In fact, the same results in Fig. 4 are obtained even when the ozonolysis reactions are excluded in the kinetic model. For this reason, ozonolysis reactions were neglected in the previous studies.

The above results demonstrate that ozone decomposition reaction occurring after the leading shock can greatly reduce the induction length. This is consistent with previous results in [3–7]. In the following, we shall consider the ozonolysis reaction taking place before the leading shock.

To quantify the ozonolysis reaction in the fresh mixture before the leading shock, we introduce the reaction progress variable,  $c = t/\tau_1$ , in which  $\tau_1$  is the first-stage ignition delay time (see Fig. 2), and  $t$  is the time at which the states in the homogeneous ignition system are chosen. The states including temperature, pressure and mixture composition are specified as the initial states to calculate the ZND detonation structure.

The influence of the reaction progress variable on the ZND detonation structure for  $\text{C}_2\text{H}_4/\text{O}_2/\text{O}_3/\text{Ar}$  mixture with  $a = 0.05$  is shown in Fig. 5. With the increase of reaction progress variable, the thermicity profile slightly moves towards the leading shock, resulting in shorter induction length. According to the results in Fig. 5, the induction length equals to  $164.2 \mu\text{m}$  for  $c = 0$ . When  $c$  is increased to 0.96, the induction length is  $150.1 \mu\text{m}$  and it is reduced by 8.6%. When  $c$  is increased to 3.2, the induction length is  $141.2 \mu\text{m}$  and it is reduced by 16.3%. The concentrations of  $\text{O}_3$  and  $\text{CH}_2\text{O}$  in the induction zone are shown to strongly depend on the reaction progress variable. This is because  $\text{O}_3$  is consumed and  $\text{CH}_2\text{O}$  is generated by the ozonolysis reaction occurring at room temperature before the leading shock. Therefore, Fig. 5 clearly demonstrates that the increasing

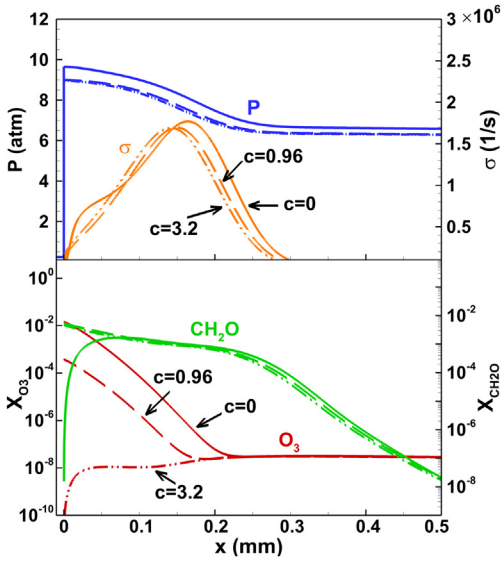


Fig. 5. Profiles for pressure,  $P$ , thermicity,  $\sigma$ , and  $O_3$  and  $CH_2O$  molar fractions,  $X_{O_3}$  and  $X_{CH_2O}$ , in the ZND detonation structure of  $C_2H_4/O_2/Ar$  mixtures with the same ozone addition of  $a = 0.05$  but different reaction progress variables.

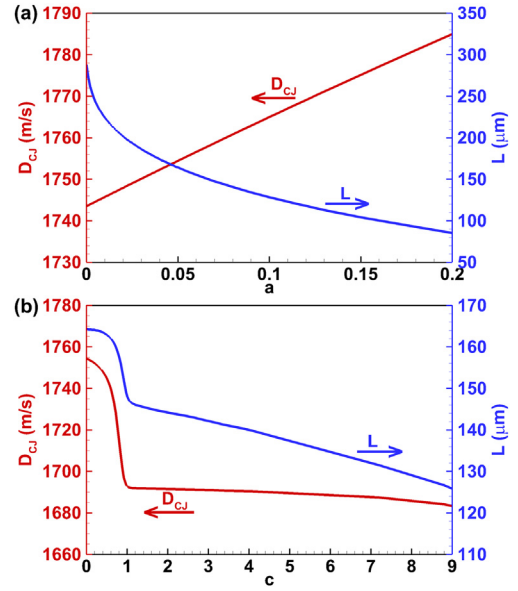


Fig. 7. Change of CJ speed,  $D_{CJ}$ , and induction length,  $L$ , with (a) the amount of ozone addition for  $c = 0$  and (b) the reaction progress variable for  $a = 0.05$ .

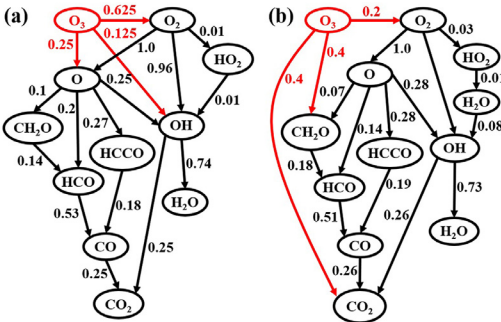


Fig. 6. Reaction path flux analysis for the ZND detonation in  $C_2H_4/O_2/Ar$  mixtures with fixed ozone addition of  $a = 0.05$  but different reaction progress variables: (a)  $c = 0$  and (b)  $c = 6.4$ . The black numbers represent the relative value of oxygen atom flux (normalized by the max oxygen flux) through various pathways and red numbers represent the percentage of ozone consumption through various pathways.

residence time before the mixture entering the leading shock/detonation can reduce the induction length due to ozonolysis reaction.

Reaction path flux analysis [28] is conducted (see Fig. 6) for the ZND detonation structure in the  $C_2H_4/O_2/O_3/Ar$  mixture with the same amount of ozone addition,  $a = 0.05$ , but different reaction progress variables. For  $c = 0$  (see Fig. 6a), there is no ozonolysis reaction occurring and ozone is mainly converted to oxygen molecule and oxy-

gen atom through the ozone decomposition reaction,  $O_3 + M = O_2 + O + M$ . Oxygen atom produced by this reaction accelerates the oxidation of  $C_2H_4$  since no chain-initiation reaction is needed. For  $c > 0$  (see Fig. 6b),  $C_2H_4$  is partially oxidized to  $CH_2O$  before the shock wave through the ozonolysis reactions listed in Eq. (1). Moreover, the ozonolysis reactions,  $C_2H_4 + O_3 = CH_2O + 2H + CO_2$  and  $C_2H_4 + O_3 = CH_2O + OH + HCO$ , respectively produce H and OH radical, which also accelerates the oxidation of  $C_2H_4$  after the shock wave.

Fig. 7 shows the change of CJ detonation speed,  $D_{CJ}$ , and the induction length,  $L$ , with the amount of ozone addition and the reaction progress variable. It is seen in Fig. 7(a) that with the increase of ozone addition,  $D_{CJ}$  increases linearly while  $L$  quickly decreases. Note the relative change in  $D_{CJ}$  is within 2%, which is almost negligible. This is because  $D_{CJ}$  is proportional to the square root of total heat release,  $Q$ , while small amount of ozone addition has little influence on  $Q$ . However, for  $a = 5\%$ , the induction length is reduced by 42.06% compared with  $a = 0$ . This is because ozone addition can greatly accelerate the ignition process through the ozone decomposition reaction which produces reactive atomic oxygen.

Fig. 7(b) shows that both  $D_{CJ}$  and  $L$  decrease with the reaction progress variable  $c$ . According to Fig. 2, the first-stage ignition caused by ozonolysis reaction has a small amount of heat release. This explains the abrupt decrease of detonation speed around  $c = 1$  in Fig. 7(b). When  $c > 1$ , the detonation speed remains nearly constant while the induc-

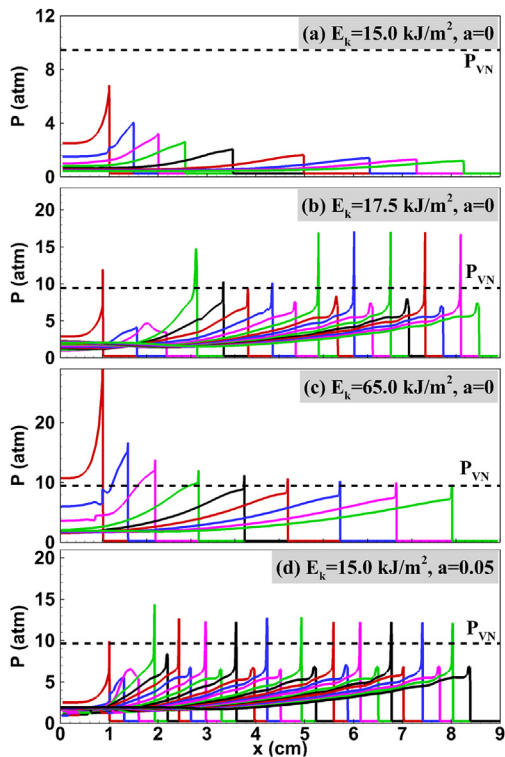


Fig. 8. Temporal evolution of pressure distributions at three initiation energies corresponding to (a) supercritical case with  $a = 0$ , (b) critical case with  $a = 0$ , (c) subcritical cases with  $a = 0$ , and (d) critical case with  $a = 0.05$  and  $c = 0$ . The dashed line denotes pressure of von Neumann spike,  $P_{VN} = 9.46$  atm.

tion time continuously decreases. This is because there is little heat release while radical is continuously produced during the period between the first and second stage ignition.

The above results demonstrate that ozonolysis reaction and ozone decomposition reaction both affect the ZND detonation structure. They are expected to affect direct detonation initiation and pulsating instability as shown in the next subsection.

### 3.3. Direct detonation initiation and propagation

First, we consider direct detonation initiation without ozone addition. Fig. 8(a-c) plots the evolution of pressure distributions for three initiation energies,  $E_k = 15$ , 17.5 and 65 kJ/m<sup>2</sup>, respectively corresponding to the subcritical, critical and supercritical cases [24]. The leading shock speeds for these cases are shown in Fig. 9. For the subcritical case with  $E_k = 15$  kJ/m<sup>2</sup>, Fig. 8(a) shows that the peak pressure continuously decreases as the shock propagates to the right side. As shown by the solid blue line in Fig. 9 for  $E_k = 15$  kJ/m<sup>2</sup> and  $a = 0$ , the lead-

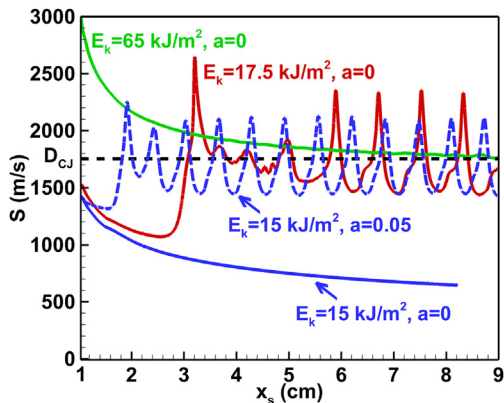


Fig. 9. Leading shock speed,  $S$ , as a function of its position,  $x_s$ , for different operating conditions. The dashed line corresponds to the CJ detonation speed,  $D_{CJ} = 1758$  m/s.

ing shock speed monotonically decreases with the shock position. The reaction front is left behind the shock wave and the distance between them continuously increases. Consequently, the reaction front decouples with the shock wave and detonation initiation fails.

For the critical case with  $E_k = 17.5$  kJ/m<sup>2</sup> shown in Fig. 8(b), the peak pressure first decreases, then increases abruptly, and finally periodic oscillation occurs. The corresponding shock speed is shown by the red line in Fig. 9. The evolution of peak pressure is similar to the change of the shock speed with the shock position as shown in Fig. 9. At the beginning, the reaction front decouples with the shock and thereby the shock speed decreases. There is a so-called “quasi-steady” period [24, 29], i.e.,  $2 < x_s < 3$  cm, during which the distance between reaction zone and shock wave keeps nearly constant and the leading shock and the reaction front propagate as a complex at nearly constant speed. At the end of the quasi-steady period, an overdriven detonation develops due to the coherent coupling between pressure pulse and chemical heat release, which can be explained by the shock wave amplification by coherent energy release (SWACER) mechanism [30, 31]. The overdriven detonation decays to a pulsating detonation whose speed oscillates around the CJ value of  $D_{CJ} = 1758$  m/s as shown in Fig. 9.

For the supercritical case with  $E_k = 65$  kJ/m<sup>2</sup>, the blast wave is shown to quickly decay toward a self-sustained CJ detonation. The temperature and heat release rate profiles (not shown here due to space limit) indicate that the reaction zone is closely coupled with the leading shock. Figs. 8 and 9 show that for  $E_k = 65$  kJ/m<sup>2</sup>, no pulsating instability appears when  $x_s < 9$  cm. This is because the stability of a 1D detonation depends crucially on the detonation velocity and the detonation is more stable at higher overdrive [32].

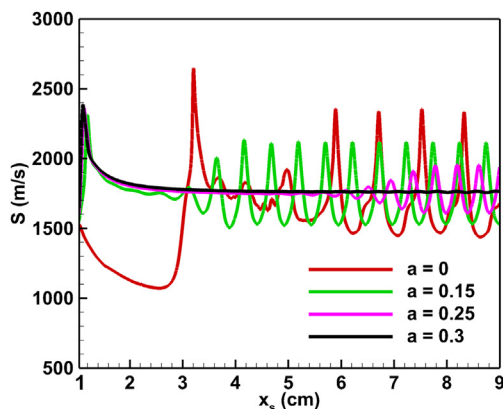


Fig. 10. Leading shock speed,  $S$ , as a function of its position,  $x_s$ , for different amounts of ozone addition. The initiation energy is fixed to be  $E_k = 17.5$  kJ/m<sup>2</sup> and  $c = 0$ .

Then, we assess the effects of ozone addition on the direct detonation initiation. Fig. 8(d) shows the results for  $E_k = 15$  kJ/m<sup>2</sup> and  $a = 0.05$ , for which the shock speed is also shown by the dashed blue line in Fig. 9. Unlike the case without ozone addition ( $E_k = 15$  kJ/m<sup>2</sup> and  $a = 0$ ) shown in Fig. 8(a), Fig. 8(d) shows that successful detonation initiation is achieved with ozone addition. Therefore, ozone addition does promote detonation initiation. Ng and Lee [29] showed that for planar geometry, the critical initiation energy is proportional to the induction length. Since ozone addition reduces the induction length (see Fig. 7a), it can also reduce the critical detonation initiation energy as demonstrated by Fig. 8(a) and 8(d).

We also examine how the amounts of ozone addition affect the direction detonation initiation and propagation. Fig. 10 shows the leading shock speed with its position for different amounts of ozone addition, ranging from  $a = 0$  to  $a = 0.3$ . The case without ozone addition, i.e.,  $a = 0$ , is also shown for comparison. Note the initiation energy is  $E_k = 17.5$  kJ/m<sup>2</sup> so that successful detonation initiation is achieved even for the case without ozone addition. Fig. 10 shows that for the cases of  $a = 0, 0.15$  and  $0.25$ , the direct detonation initiation results in pulsating detonation whose shock speed oscillates around the CJ value. It is noticed that the amplitude of the oscillation decreases with the amount of ozone addition. For  $a = 0.3$ , there is no oscillation in Fig. 10 and stable detonation propagation is achieved. Besides, Fig. 10 shows that for the case without ozone addition (i.e.,  $a = 0$ ), the overdriven detonation first appears at  $x_s = 3.2$  cm. However, for the case with ozone addition (i.e.,  $a = 0.15, 0.25$  and  $0.3$ ), the overdriven detonation appears immediately. Certainly, the appearance of the overdriven detonation depends on both the initiation energy and the amount of ozone addition. With the in-

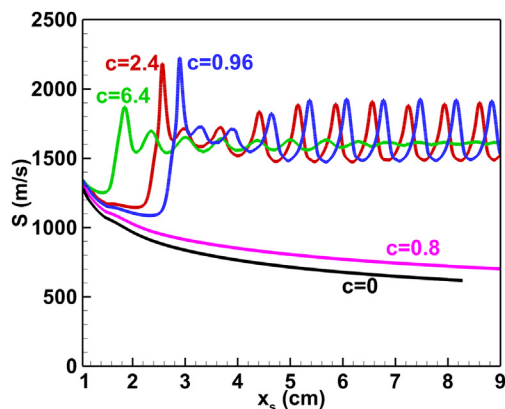


Fig. 11. Leading shock speed,  $S$ , as a function of its position,  $x_s$ , for different reaction progress variables. The initiation energy is fixed to be  $E_k = 12$  kJ/m<sup>2</sup> and  $a = 0.05$ .

crease of initiation energy or ozone addition, the overdriven detonation appears earlier.

For the results shown in Figs. 8–10, the reaction progress variable is zero, i.e.,  $c = 0$ . Therefore, there is no ozonolysis reaction involved. To assess the influence of ozonolysis reaction on direct detonation initiation and propagation. We fix the initiation energy,  $E_k = 12$  kJ/m<sup>2</sup>, and the amount of ozone addition,  $a = 0.05$ , but change the reaction progress variable  $c$ . The results are depicted in Fig. 11.

Fig. 11 shows for  $c = 0$  and  $c = 0.8$ , the leading shock speed,  $S$ , decays monotonically, indicating that detonation initiation fails. According to the definition of the reaction progress variable,  $c = t/\tau_1$  (where  $\tau_1$  is the first-stage ignition delay time shown in Fig. 2), the radical/thermal runaway caused by ozonolysis reaction is still not fully developed for  $c = 0.8 < 1$ . When the reaction progress variable increases to  $c = 0.96 < 1$ , Fig. 11 shows that successful direct detonation initiation is achieved and a pulsating detonation develops afterwards. The overdriven detonation is generated at  $x_s = 2.8$  cm for  $c = 0.96$ . When the reaction progress variable increases to  $c = 2.4$ , the shock speed evolution remains to be similar to that for  $c = 0.96$  while the position for the generation of the overdriven moves to  $x_s = 2.5$  cm. For very large reaction progress variable of  $c = 6.4$ , Fig. 11 shows that the overdriven detonation develops much earlier at  $x_s = 1.9$  cm. This indicates that the detonation can be more easily initiated at larger reaction progress variable. Therefore, the above results demonstrate that the ozonolysis reaction does promote detonation initiation in C<sub>2</sub>H<sub>4</sub>/O<sub>2</sub>/O<sub>3</sub>/Ar mixtures.

Fig. 11 also shows that the detonation stability increases with the reaction progress variable. For  $c = 0.96$  and  $c = 2.4$ , oscillation of the shock speed is clearly shown in Fig. 11. However, for  $c = 6.4$ , the oscillation gradually decays and finally stable

detonation propagation is achieved. Therefore, the ozonolysis reactions also improve the detonation stability for  $C_2H_4/O_2/O_3/Ar$  mixtures.

The above results demonstrate that increasing the amount of ozone addition and/or the reaction progress variable not only makes the direct detonation initiation easier but also makes the detonation propagation more stable. Since the critical initiation energy is proportional to the induction length for planar geometry [29], the above effects of on direct detonation initiation can be easily interpreted by the change of the induction length with ozone addition and reaction progress variable as shown in Fig. 7. The above effects on detonation stability can be interpreted with the help of Lee and Stewart's theory [32]. Their theory indicates that detonation stability is mainly determined by the degree of detonation overdrive, non-dimensional activation energy, non-dimensional heat release, and specific heat ratio, which has been verified in the paper of Yungster et al. [33]. The degree of detonation overdrive is mainly affected by the initiation energy, and its influence disappears as the detonation speed decays to the CJ value. Simple calculation shows that the non-dimensional heat release and specific heat ratio do not change obviously with ozone addition and reaction progress variable. Therefore, the change of detonation stability is mainly due to the change in the non-dimensional activation energy caused by ozone addition and/or ozonolysis reaction.

The non-dimensional activation energy,  $\theta$ , can be calculated according to Daimon et al. [34]:

$$\theta = \frac{E}{RT_S} = \frac{1}{T_S} \frac{\ln(t_{i1}) - \ln(t_{i2})}{(1/T_1 - 1/T_2)} \quad (3)$$

$$T_1 = 1.01T_S, \quad T_2 = 0.99T_S$$

where  $T_S$  is the temperature behind the shock wave and  $t_i$  is the induction time. The effects of ozone addition and ozonolysis reaction on the non-dimensional activation energy are shown in Fig. 12. It is seen that increasing the amount of ozone addition,  $a$ , and increasing the reaction progress variable,  $c$ , can both reduce the non-dimensional activation energy,  $\theta$ . Consequently, according to Lee and Stewart's theory [32] the detonation stability can be improved by increasing  $a$  and  $c$ . This explains why pulsating instability disappears for large values of  $a$  and  $c$ , as shown in Figs. 10 and 11. The reduction of activation energy can also be interpreted by chemical kinetics.

#### 4. Conclusions

Numerical simulations are conducted to assess the effects of ozone addition and ozonolysis reaction on steady detonation structure and transient direct detonation initiation and propagation processes in  $C_2H_4/O_2/O_3/Ar$  mixtures. First, the ho-

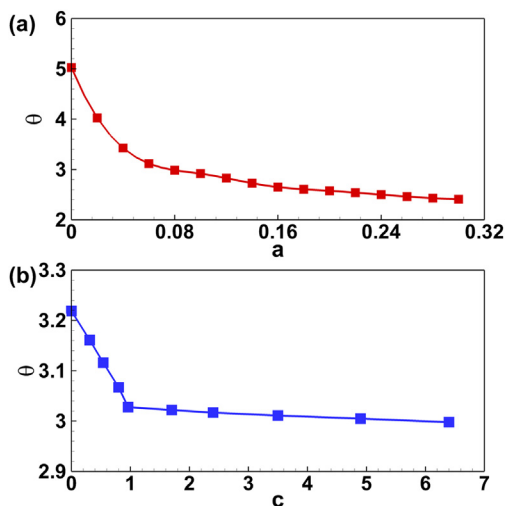


Fig. 12. Change of the non-dimensional activation energy,  $\theta$ , with (a) the amount of ozone addition,  $a$ , for fixed  $c = 0$  and (b) reaction progress variable,  $c$  for fixed  $a = 0.05$ .

mogeneous ignition process is investigated. The ignition process is found to consist of two stages and the first stage is caused by ozonolysis reactions which consume  $O_3$  and produce  $CH_2O$  as well as H and OH radicals. Then, the ZND detonation structure is considered. It is demonstrated that ozonolysis reaction and ozone decomposition reaction can both reduce the induction length while have little influence on the CJ detonation speed. Finally, the transient direct detonation initiation and propagation are studied. It is found that increasing the amount of ozone addition and/or the reaction progress variable not only makes the direct detonation initiation easier but also makes the detonation propagation more stable. The change in critical initiation energy is interpreted by the change of the induction length with ozone addition and reaction progress variable; while the increase of detonation stability is mainly attributed to the reduction in the non-dimensional activation energy caused by ozone addition and/or ozonolysis reaction. The present results indicate that both ozone decomposition reaction and ozonolysis reaction can enhance detonation for unsaturated hydrocarbon fuels.

Here only one-dimensional simulations are conducted. In future works, it would be interesting to conduct multi-dimensional simulations and to assess the effects of ozone addition and ozonolysis reactions on detonation dynamics of  $C_2H_4/O_2/O_3/Ar$  mixtures. As mentioned before, the double peaks in the thermicity profile caused by ozone addition may induce double detonation cellular structure as reported in [27]. Besides, the progress of ozonolysis reactions occurring in  $C_2H_4/O_2/O_3/Ar$  mixtures strongly depends on the mixing time and reactiv-

ity non-uniformity might be induced by imperfect mixing of O<sub>3</sub> with the mixtures. The inhomogeneity in mixture composition (i.e., different amounts of O<sub>3</sub> addition) and inhomogeneity reaction progress variable (i.e., different progresses of ozonolysis reaction) both can greatly affect the detonation initiation and cellular structure, which deserves further studies. Here we only consider one type of unsaturated hydrocarbon, ethylene. It is of interests to study how ozone addition and ozonolysis reactions affect the detonation of different unsaturated hydrocarbons in future works.

### Declaration of Competing Interest

The authors declare that they have no known competing financial interests or personal relationships that could have appeared to influence the work reported in this paper.

### Acknowledgments

This work was supported by National Natural Science Foundation of China (Nos. 52176096 and 52006001). We thank the help on reaction path flux analysis by Dr. Yiqing Wang at Peking University.

### Supplementary materials

Supplementary material associated with this article can be found, in the online version, at doi:10.1016/j.proci.2022.09.029.

### References

- [1] P. Wolański, Detonative propulsion, *Proc. Combust. Inst.* 34 (2013) 125–158.
- [2] W. Sun, X. Gao, B. Wu, T. Ombrello, The effect of ozone addition on combustion: kinetics and dynamics, *Prog. Energy Combust. Sci.* 73 (2019) 1–25.
- [3] X. Shi, J. Crane, H. Wang, Detonation and its limit in small tubes with ozone sensitization, *Proc. Combust. Inst.* 38 (2021) 3547–3554.
- [4] J. Sepulveda, A. Rouso, H. Ha, T. Chen, V. Cheng, W. Kong, Y. Ju, Kinetic enhancement of microchannel detonation transition by ozone addition to acetylene mixtures, *AIAA J.* 57 (2019) 476–481.
- [5] W. Han, J. Huang, C. Wang, Pulsating and cellular instabilities of hydrogen–oxygen detonations with ozone sensitization, *Phys. Fluids* 33 (2021) 076113.
- [6] W. Han, W. Liang, C. Wang, J. Wen, C.K. Law, Spontaneous initiation and development of hydrogen–oxygen detonation with ozone sensitization, *Proc. Combust. Inst.* 38 (2021) 3575–3583.
- [7] D.S. Kumar, K. Ivin, A.V. Singh, Sensitizing gaseous detonations for hydrogen/ethylene-air mixtures using ozone and H<sub>2</sub>O<sub>2</sub> as dopants for application in rotating detonation engines, *Proc. Combust. Inst.* 38 (2021) 3825–3834.
- [8] S.E. Paulson, J.D. Fenske, A.D. Sen, T.W. Callahan, A novel small-ratio relative-rate technique for measuring OH formation yields from the reactions of O<sub>3</sub> with alkenes in the gas phase, and its application to the reactions of ethene and propene, *J. Phys. Chem. A* 103 (1999) 2050–2059.
- [9] J.D. Fenske, A.S. Hasson, S.E. Paulson, K.T. Kuwata, A. Ho, K.N. Houk, The pressure dependence of the OH radical yield from ozone-alkene reactions, *J. Phys. Chem. A* 104 (2000) 7821–7833.
- [10] X. Gao, B. Wu, W. Sun, T. Ombrello, C. Carter, Ozonolysis activated autoignition in non-premixed coflow, *J. Phys. D: Appl. Phys.* 52 (2019) 105201.
- [11] X. Gao, Y. Zhang, S. Adusumilli, J. Seitzman, W. Sun, T. Ombrello, C. Carter, The effect of ozone addition on laminar flame speed, *Combust. Flame* 162 (2015) 3914–3924.
- [12] C.B. Reuter, T.M. Ombrello, Flame enhancement of ethylene/methane mixtures by ozone addition, *Proc. Combust. Inst.* 38 (2021) 2397–2407.
- [13] C.J. Weschler, Ozone in indoor environments: concentration and chemistry, *Indoor Air* 10 (2000) 269–288.
- [14] X. Chen, W. Peng, P. Gillard, L. Courty, M.L. Sankhe, S. Bernard, Y. Wu, Y. Wang, Z. Chen, Effects of fuel decomposition and stratification on the forced ignition of a static flammable mixture, *Combust. Theory Model.* 25 (2021) 813–831.
- [15] Z. Luo, T. Lu, J. Liu, A reduced mechanism for ethylene/methane mixtures with excessive NO enrichment, *Combust. Flame* 158 (2011) 1245–1254.
- [16] Z.H. Wang, L. Yang, B. Li, Z.S. Li, Z.W. Sun, M. Aldén, K.F. Cen, A.A. Konnov, Investigation of combustion enhancement by ozone additive in CH<sub>4</sub>/air flames using direct laminar burning velocity measurements and kinetic simulations, *Combust. Flame* 159 (2012) 120–129.
- [17] D.G. Goodwin, R.L. Speth, H.K. Moffat, B.W. Weber, available at <https://www.cantera.org>.
- [18] S. Browne, J. Ziegler, J.E. Shepherd, available at <https://shepherd.caltech.edu/EDL/PublicResources>.
- [19] L.I. Sedov, M. Holt, M. Friedmann, Similarity and dimensional methods in mechanics, *Phys. Today* 13 (1959) 355–358.
- [20] G.I. Taylor, The formation of a blast wave by a very intense explosion, *Proc. R. Soc. Lond.* 201 (1950) 159–174.
- [21] Z. Chen, Effects of radiation and compression on propagating spherical flames of methane/air mixtures near the lean flammability limit, *Combust. Flame* 157 (2010) 2267–2276.
- [22] Z. Chen, M.P. Burke, Y. Ju, Effects of Lewis number and ignition energy on the determination of laminar flame speed using propagating spherical flames, *Proc. Combust. Inst.* 32 (2009) 1253–1260.
- [23] P. Dai, Z. Chen, Supersonic reaction front propagation initiated by a hot spot in n-heptane/air mixtures with multistage ignition, *Combust. Flame* 162 (2015) 4183–4193.
- [24] C. Qi, Z. Chen, Effects of temperature perturbation on direct detonation initiation, *Proc. Combust. Inst.* 36 (2017) 2743–2751.
- [25] P. Dai, Z. Chen, Effects of NO<sub>x</sub> addition on autoignition and detonation development in DME/air under engine-relevant conditions, *Proc. Combust. Inst.* 37 (2019) 4813–4820.

- [26] Y. Wang, C. Huang, R. Deiterding, H. Chen, Z. Chen, Propagation of gaseous detonation across inert layers, *Proc. Combust. Inst.* 38 (2021) 3555–3563.
- [27] F. Joubert, D. Desbordes, H.N. Presles, Detonation cellular structure in  $\text{NO}_2/\text{N}_2\text{O}_4$ -fuel gaseous mixtures, *Combust. Flame* 152 (2008) 482–495.
- [28] W. Sun, Z. Chen, X. Gou, Y. Ju, A path flux analysis method for the reduction of detailed chemical kinetic mechanisms, *Combust. Flame* 157 (2010) 1298–1307.
- [29] H.D. Ng, J.H.S. Lee, Direct initiation of detonation with a multi-step reaction scheme, *J. Fluid Mech.* 476 (2003) 179–211.
- [30] J.H.S. Lee, R. Knystautas, N. Yoshikawa, Photochemical initiation of gaseous detonations, *Acta Astronaut.* 5 (1978) 971–982.
- [31] J.H.S. Lee, *The Detonation Phenomenon*, Cambridge University Press, Cambridge, 2008.
- [32] H.I. Lee, D.S. Stewart, Calculation of linear detonation instability: one-dimensional instability of plane detonation, *J. Fluid Mech.* 216 (1990) 103–132.
- [33] S. Yungster, K. Radhakrishnan, Structure and stability of one-dimensional detonations in ethylene-air mixtures, *Shock Waves* 14 (2005) 61–72.
- [34] Y. Daimon, A. Matsuo, Unsteady features on one-dimensional hydrogen-air detonations, *Phys. Fluids* 19 (2007) 116101.